Effect of small particles on low Reynolds number turbulent channel in four-way coupled DNS

Fan Zhao
Amanda Sjödahl
Berend Van Wachem
Mechanical Engineering, Imperial College

William K. George
Aeronautics, Imperial College

Low Re Simulation set-up

- Dimensions: $2\pi h \times 4\pi h \times 2h$
- $Re_\tau = 150$
- Flow driven by pressure drop (source term) to sustain channel flow.

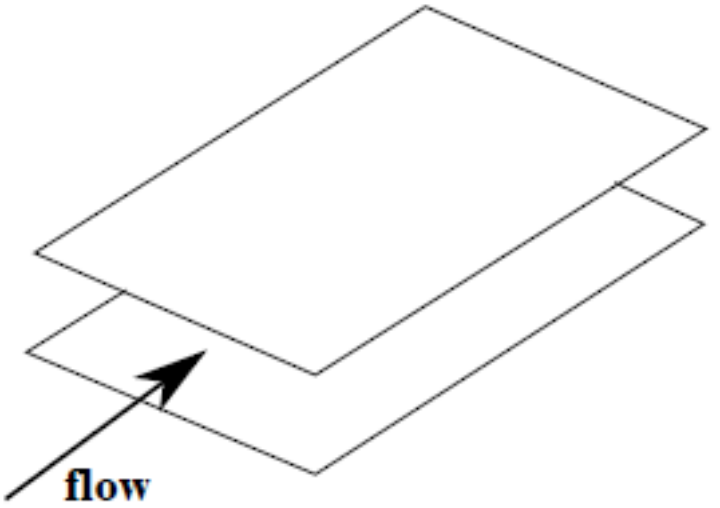

Marchioli, C., *et al.* (2008). Int J of Multiphase Flow, 34(9), 879-93.

PARTICLE SHAPES

shape	sphericity	proportions	size
sphere	1		$d = 200\,\mu m$
			
ellipsoid	0.88	$\frac{a}{b} = \frac{5}{2}$	$a = 368\,\mu m \;\; b = 147\,\mu m$
			
fiber	0.70	$\frac{a}{b} = 5$	$a = 510\,\mu m \;\; b = 102\,\mu m$
			
disc	0.88	$\frac{a}{b} = 5$	$a = 350\,\mu m \;\; b = 70\,\mu m$
			

Particle 'body space' vs. 'world (or fluid) space'

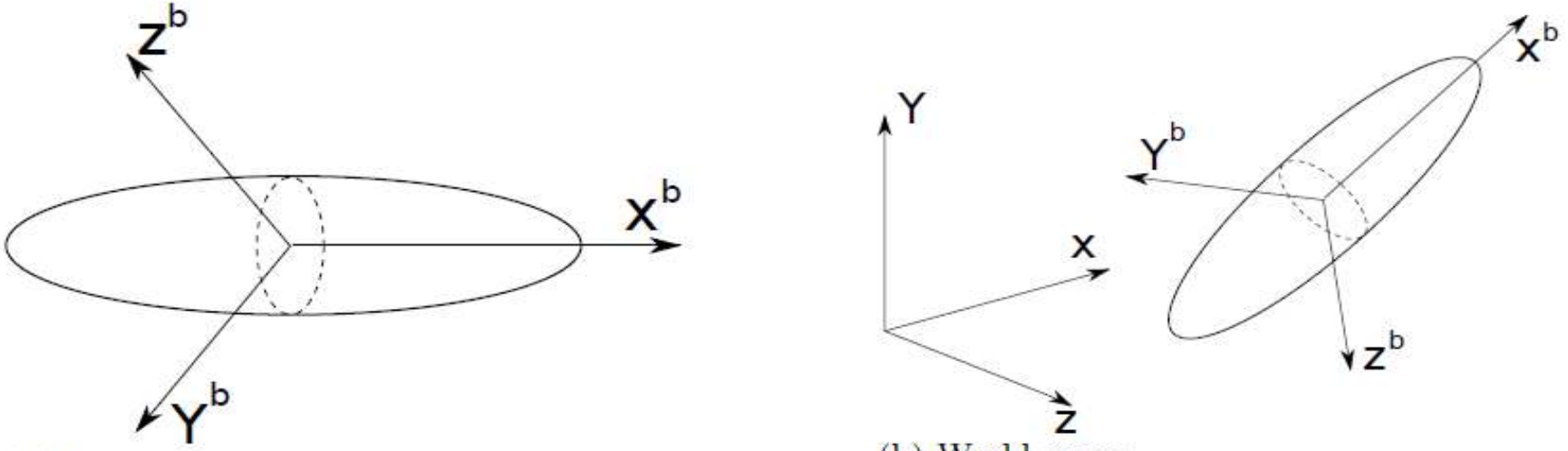

(a) Body space (b) World space

Fig. 1 (a) Body space and (b) World space co-ordinates. The x^b axis of the body-space co-ordinate system always aligns with the major-axis of the ellipsoidal particle, whereas the world-space co-ordinates remain fixed in space and time.

The translational motion of particles is governed by the Newton's second law in world space,

$$\sum \boldsymbol{F} = m\frac{d\boldsymbol{u}^P}{dt} \tag{4}$$

where $\sum \boldsymbol{F}$ is the resultant external force on the particle, m is the particle mass, and $\boldsymbol{u}^P$ represents the particle translational velocity. Due to the applied assumptions and large particle-fluid density ratio, several forces in the Basset-Boussinesq-Oseen (BBO) equation [13, 34] are neglected in this work, and only hydrodynamic drag, the pressure gradient and collision forces are included in $\sum \boldsymbol{F}$.

For non-spherical particles, the representation of the rotation requires a rotation operator. There are three most commonly used operators to describe rotation dynamics: Euler angles, rotation matrices, and unit Quaternions. Applying the former two can give rise to gimbal lock and singularity problems [17], and hence the latter, unit Quaternions, are used in this study. A Quaternion can be defined as:

$$q = [q_0, \boldsymbol{q}] \tag{7}$$

where q_0 is a scalar number, and $\boldsymbol{q} = [q_1,\ q_2,\ q_3]$ is a vector. In dynamic systems, a general Quaternion cannot only rotate a vector, but also scale the length of the vector, *e.g.* [23]. To describe rotation without scaling, the length of Quaternions must always be 1, given as:

$$|q| = \sqrt{q_0^2 + q_1^2 + q_2^2 + q_3^2} = 1 \tag{8}$$

Furthermore, the Quaternion multiplication product is required, which can be defined as:

$$pq = [p_0 q_0 - \boldsymbol{pq}, p_0 \boldsymbol{q} + q_0 \boldsymbol{p} + \boldsymbol{p} \times \boldsymbol{q}] \tag{9}$$

where p and q are Quaternions.
A vector $\boldsymbol{v}$ rotated by a pair of unit Quaternions is defined by

$$\boldsymbol{v}'' = q v q^{-1} \tag{10}$$

where $q^{-1} = [q_0, -\boldsymbol{q}]$ represents the conjugation of q, and vector $\boldsymbol{v}$ is interpreted as the Quaternion, $[0, \boldsymbol{v}]$.

In the literature, most integration methods for updating unit Quaternions are performed based on Taylor expansions, *e.g.* [1, 6, 27, 37, 44]. Unfortunately, these algorithms cannot preserve the unit length of the rotation operators; therefore, the Quaternions must be re-normalized after each particle time-step. Although the re-normalization procedure ensures that the Quaternions keep their unit lengths, the inherent relationship among the 4 components in a Quaternion is affected and leads to inevitable errors in rotation angle. To avoid this, this study employs a new algorithm PCDM method [48] to integrate unit Quaternions. This method implicitly preserves the length of unit Quaternions without re-normalization. The unit Quaternion at the next time-level $n+1$ is determined by

$$q_{n+1} = \tilde{q}_{n+1} q_n \tag{14}$$

where the unit Quaternion $\tilde{q}_{n+1}$ represents the rotation from time-level n to $n+1$ and is defined by

$$\tilde{q}_{n+1} = \left[\cos\left(\frac{|\boldsymbol{\omega}_{n+\frac{1}{2}}|\delta t}{2}\right), \sin\left(\frac{|\boldsymbol{\omega}_{n+\frac{1}{2}}|\delta t}{2}\right) \frac{\boldsymbol{\omega}_{n+\frac{1}{2}}}{|\boldsymbol{\omega}_{n+\frac{1}{2}}|} \right] \tag{15}$$

where δt represents the time-step, and $|\boldsymbol{\omega}_{n+\frac{1}{2}}|$ is the length of angular velocity $\boldsymbol{\omega}_{n+\frac{1}{2}}$. In Equation 14, the multiplication product between two unit Quaternions guarantees the unit length of the results q_{n+1}. In the PCDM algorithm, the angular velocity of particles and unit Quaternions are approximated by a predictor-corrector method. Firstly, the external torque $\boldsymbol{T}_n$ and angular velocity $\boldsymbol{\omega}_n$ of a particle are transformed from world space to body space using Equation 10, and temporal $\boldsymbol{\omega}^b_{n+\frac{1}{4}}$ and $\boldsymbol{\omega}^b_{n+\frac{1}{2}}$ in body space are then computed by the first order Euler algorithm. After that, a predictor Quaternion $q''_{n+\frac{1}{2}}$ can be determined by

$$q''_{n+\frac{1}{2}} = \left[\cos\frac{\|\boldsymbol{\omega}_{n+\frac{1}{4}}\|\delta t}{4}, \sin\frac{\|\boldsymbol{\omega}_{n+\frac{1}{4}}\|\delta t}{4} \frac{\boldsymbol{\omega}_{n+\frac{1}{4}}}{\|\boldsymbol{\omega}_{n+\frac{1}{4}}\|} \right] q_n \tag{16}$$

Applying $q''_{n+\frac{1}{2}}$, $\boldsymbol{\omega}^b_{n+\frac{1}{2}}$ is transformed to world space to determine $\tilde{q}_{n+1}$ in Equation 14. Finally, the unit Quaternion q_{n+1} and $\boldsymbol{\omega}^b_{n+1}$ are updated. Further details can be found in [48].

Forces and Torques on a particle

Drag Force

$$F_d = C_D(\ldots)\frac{1}{2}\rho_g\frac{\pi}{4}d_p^2(\tilde{v}_f - v_p)^2$$

Lift Force

$$F_l = C_L(\ldots)\frac{1}{2}\rho_g\frac{\pi}{4}d_p^2(\tilde{v}_f - v_p)^2$$

Aerodynamic Torque

$$T_{aero} = C_T(\ldots)\frac{1}{2}\rho_g\frac{\pi}{8}d_p^3(\tilde{v}_f - v_p)^2$$

Rotational Torque

$$T_{rot} = C_R(\ldots)\frac{\rho}{2}\left(\frac{d_p}{2}\right)^5|\omega_p|\omega_p$$

Results: DNS Simulations

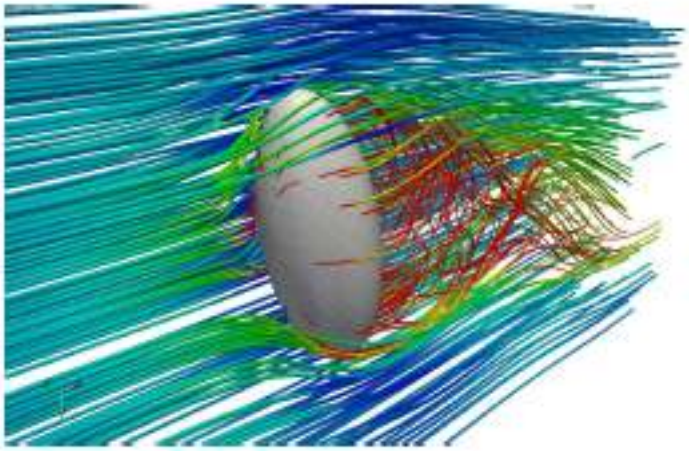

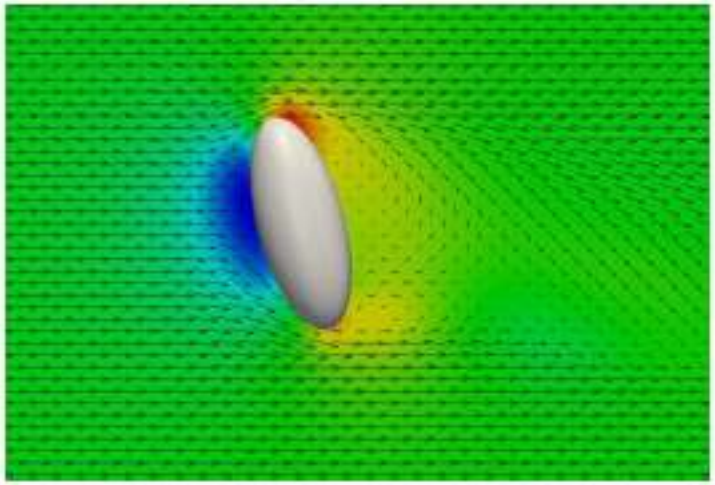

$$C_D(\varphi) = C_{D,\varphi=0^o} + (C_{D,\varphi=90^o} - C_{D,\varphi=0^o}) sin^{a_0}\varphi$$

$$C_{D,\varphi=0^o} = \frac{a_1}{Re^{a_2}} + \frac{a_3}{Re^{a_4}}$$

$$C_{D,\varphi=90^o} = \frac{a_5}{Re^{a_6}} + \frac{a_7}{Re^{a_8}}$$

$$C_L = \left(\frac{b_1}{Re^{b_2}} + \frac{b_3}{Re^{b_4}}\right) sin(\varphi)^{b_5+b_6 Re^{b_7}} cos(\varphi)^{b_8+b_9 Re^{b_{10}}}$$

$$C_T = \left(\frac{c_1}{Re^{c_2}} + \frac{c_3}{Re^{c_4}}\right) sin(\varphi)^{c_5+c_6 Re^{c_7}} cos(\varphi)^{c_8+c_9 Re^{c_{10}}}$$

Imperial College London

Zastawny et al. (2012)

COLLISION DYNAMICS FOR NON-SPHERICAL

contacts are found through "spheres":

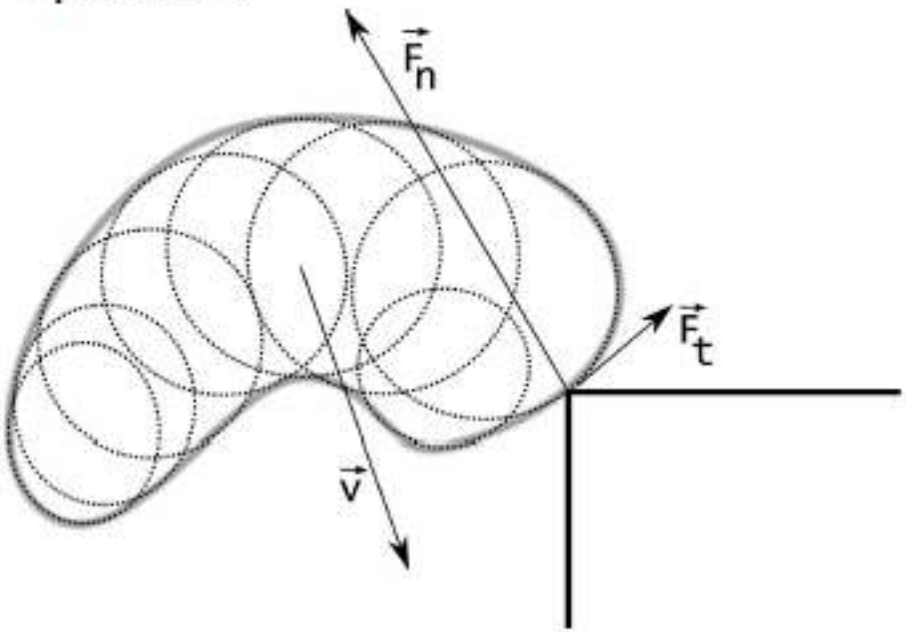

Hertzian contact model:

"fixed" time-step

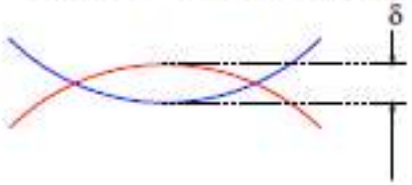

$$F_n(t) = K_n(t)\delta_n^{\frac{3}{2}}(t)n(t)$$

$$F_t(t) = min(\mu F_n(t), K_t(t)\delta_t(t))$$

St	λ	ρ $[kg/m^3]$	minor-axis $(a)[\mu m]$	Major-axis (b) $[\mu m]$	numbers (N)	Volume fraction [%]
5.0	1.0	225.68	96.0	96.0	200,000	0.0073
30	1.0	1354.21	96.0	96.0	200,000	0.0073
5.0	3.0	120.77	96.0	287.93	200,000	0.022
30.0	3.0	724.23	96.0	287.93	200,000	0.022
5.0	5.0	93.7	96.0	480.0	200,000	0.036
30.0	5.0	578.77	96.0	480.0	200,000	0.036

Table 3 The properties of the particles used in the simulations

The Results (Mean Velocity)

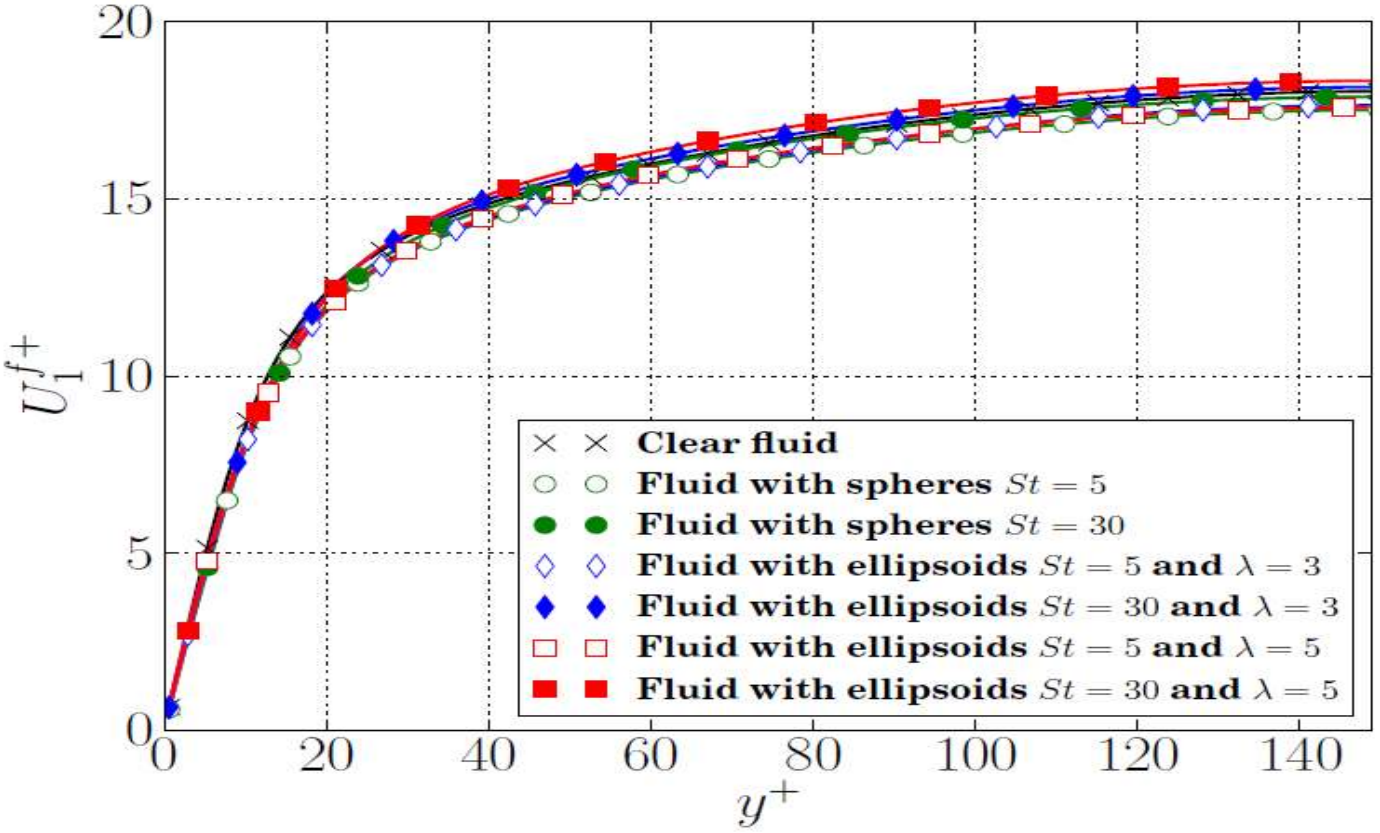

- The wall shear stress is exactly the same for all plots.
- Different centerline values imply drag reduction.
- The viscosity is exactly the same also. Collapse at low yplus implies no change in viscosity.

Mean velocity:
Near wall (left) and Core (right)

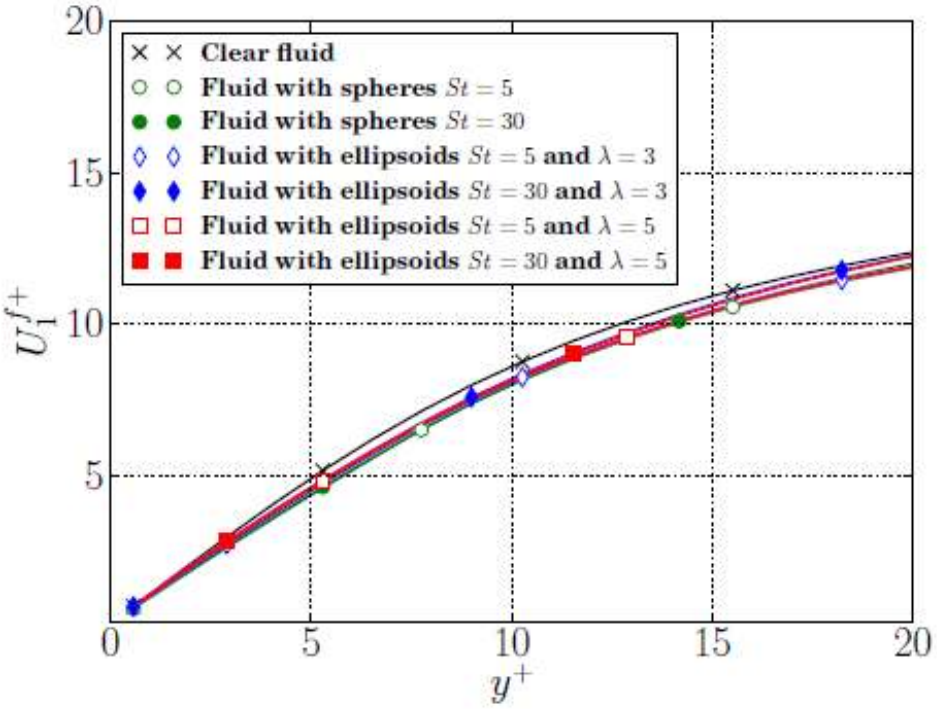

Fig. 3 Fluid mean velocity in the flow direction as a function of distance to the wall in the near wall region

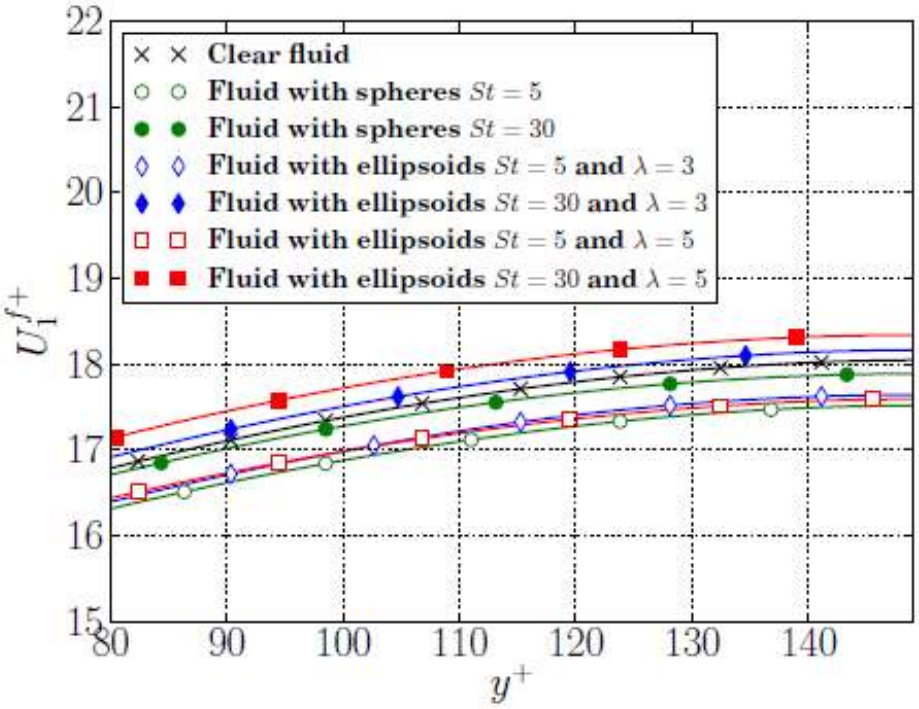

Fig. 4 Fluid mean velocity in the flow direction in the central region of the channel

RMS Streamwise Velocity

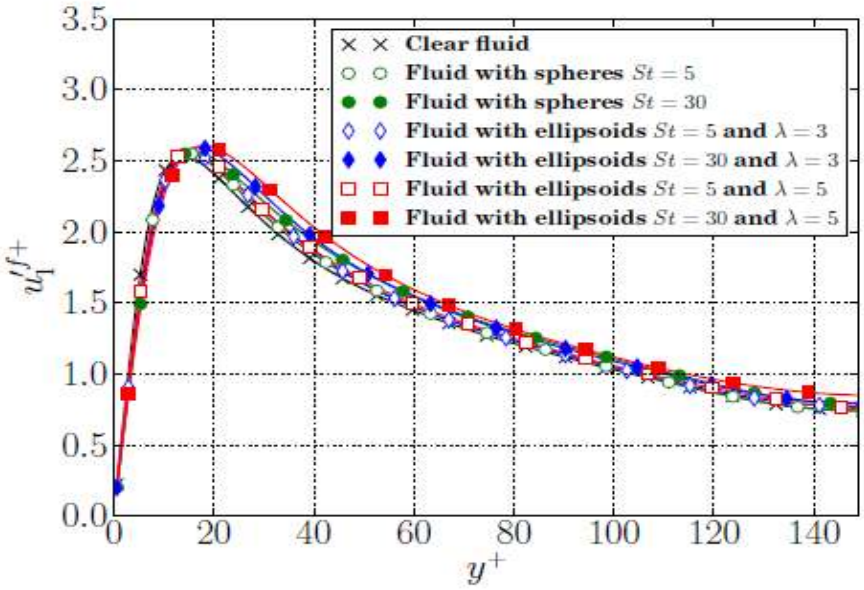

Fig. 7 Fluid RMS velocity in the stream-wise direction as a function of distance to the wall

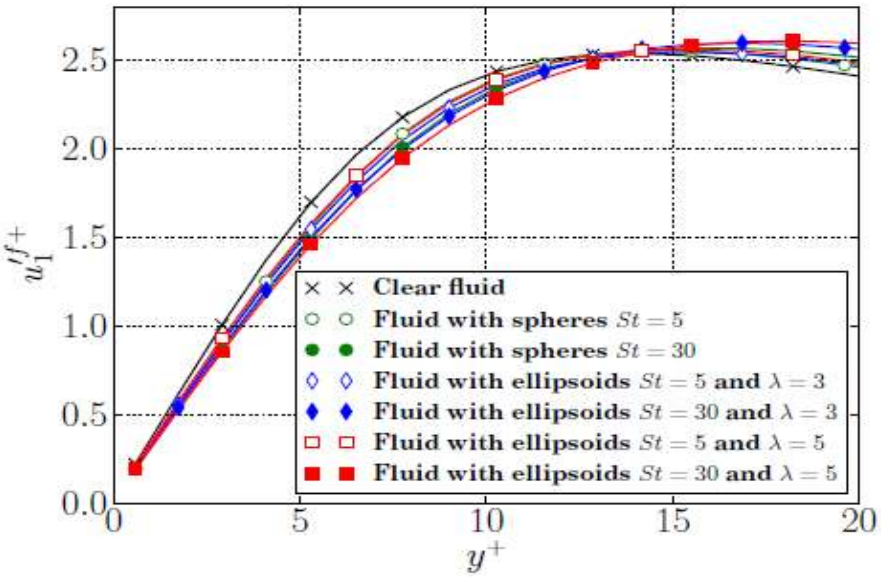

Fig. 8 Fluid RMS velocity in the stream-wise direction as a function of distance to the wall

RMS wall-normal and spanwise velocities

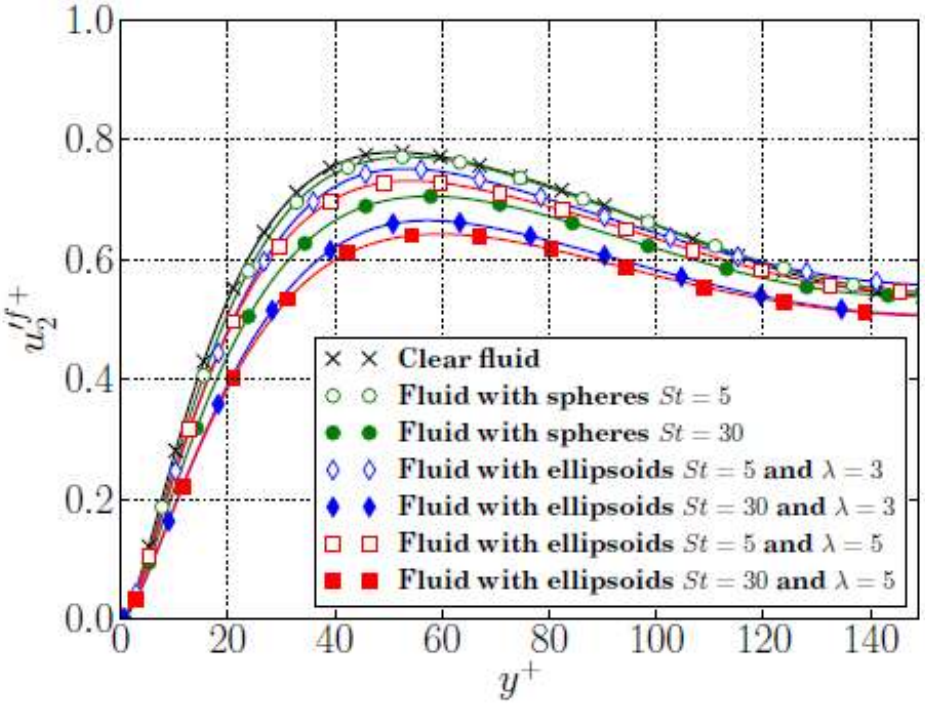

Fig. 5 Fluid RMS velocity in the wall-normal direction as a function of distance to the wall

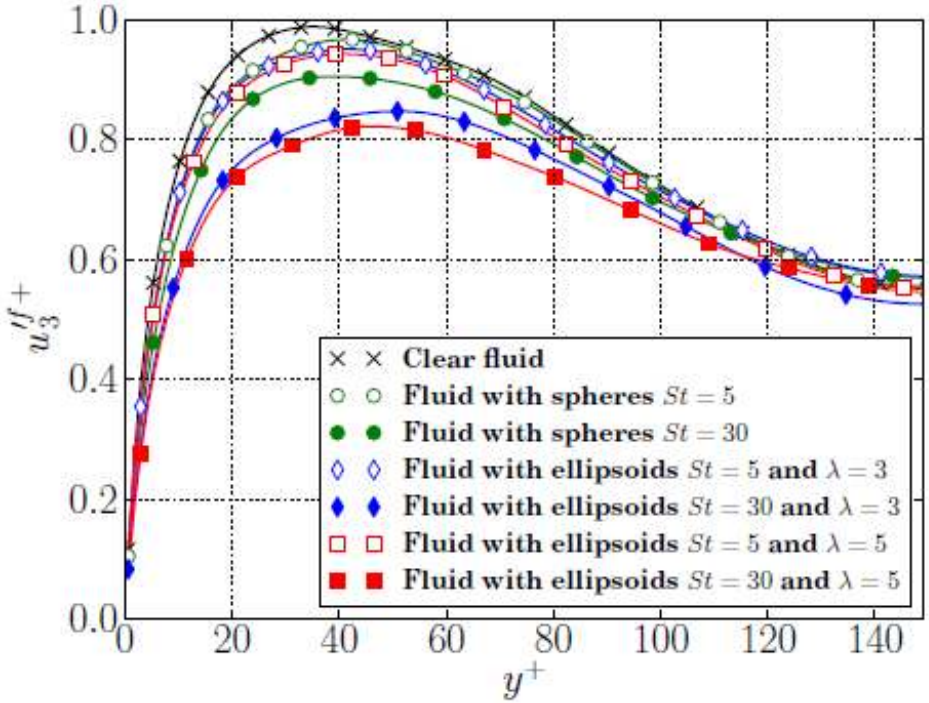

Fig. 6 Fluid RMS velocity in the span-wise direction as a function of distance to the wall

Reynolds shear stress (left) and Production (right)

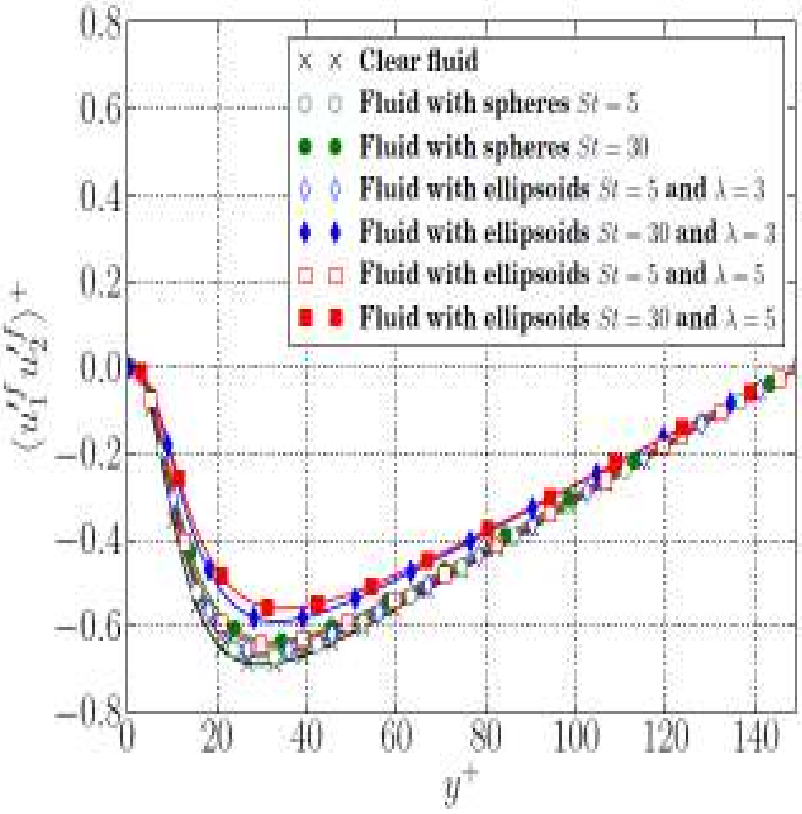

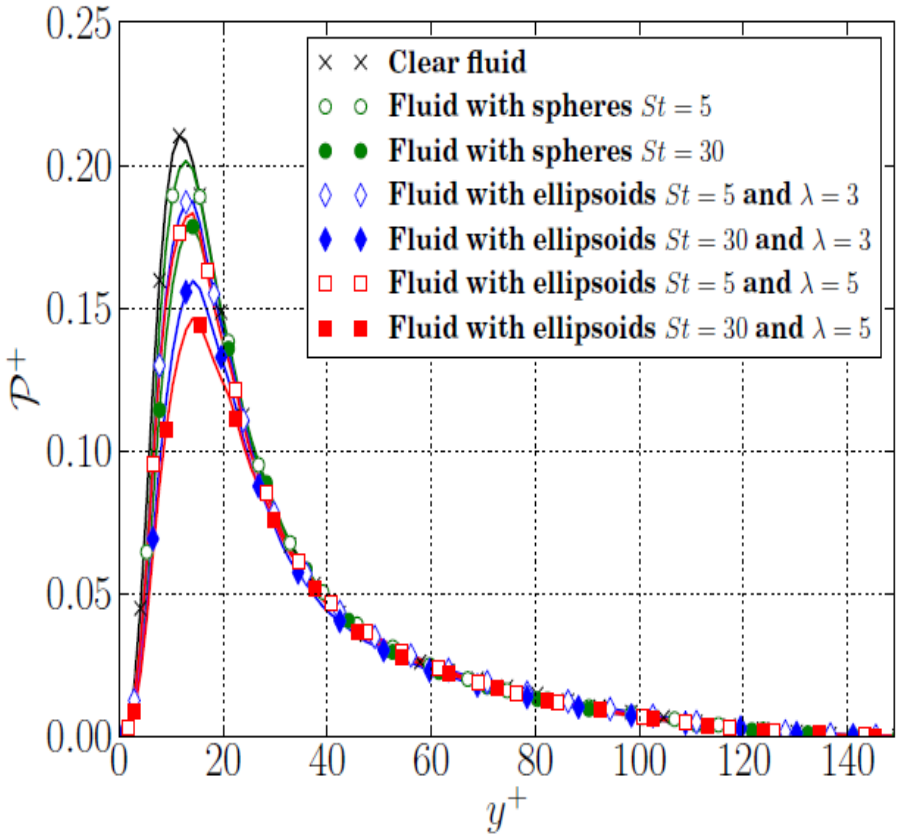

Flow dissipation (left) and particle dissipation (right).

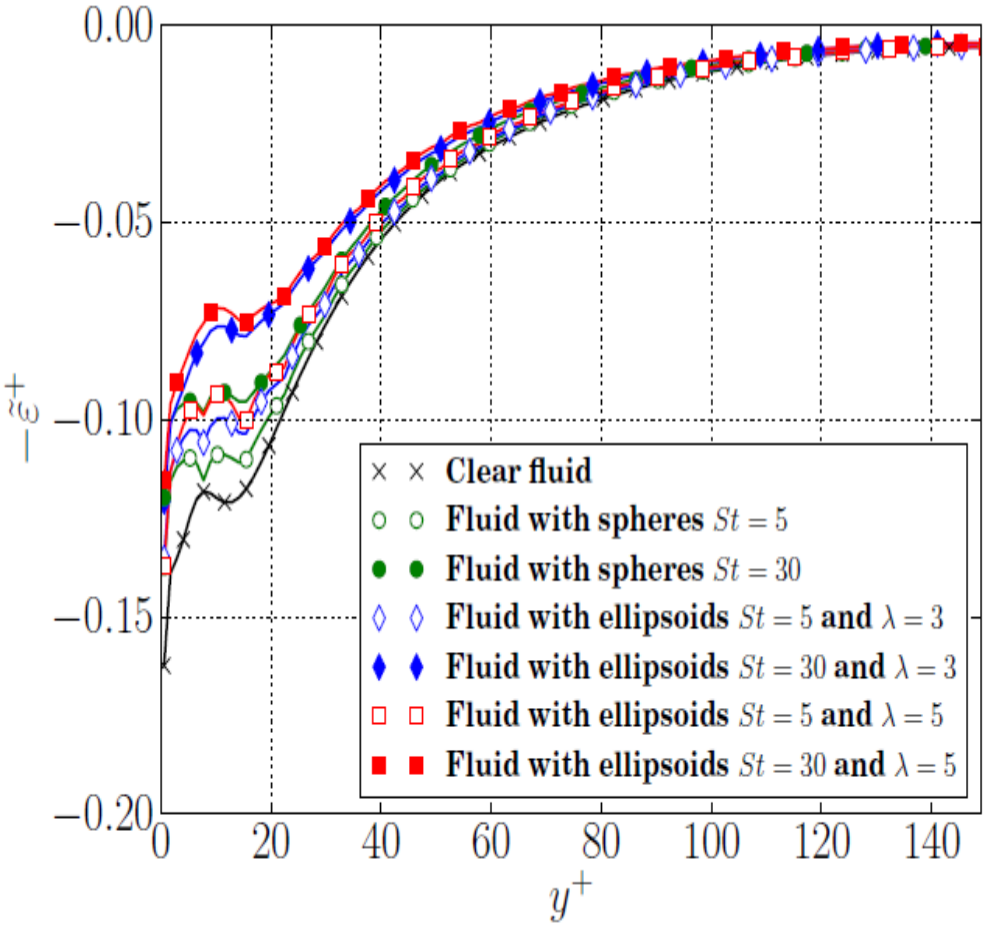

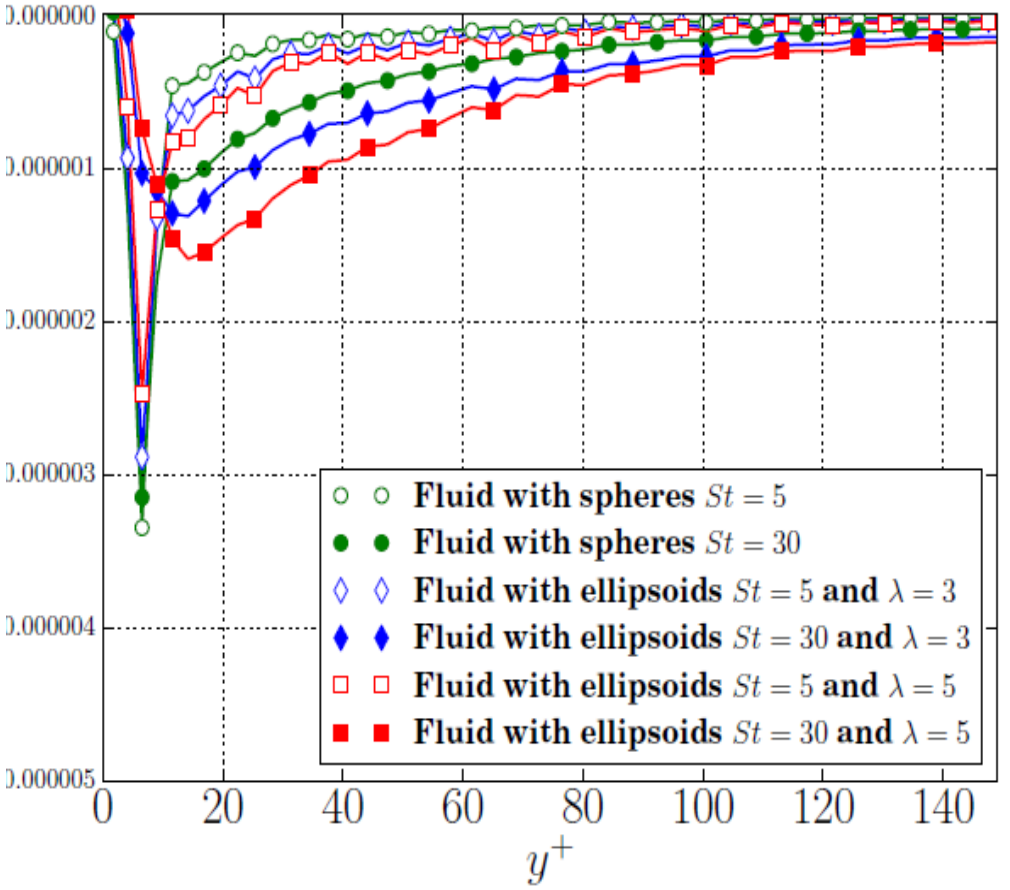

- Note right plot-scale is many orders of magnitude less. So particle dissipation negligible.

Three main velocity derivatives contribute to dissipation

- Two of them differ

  a lot very near the wall.

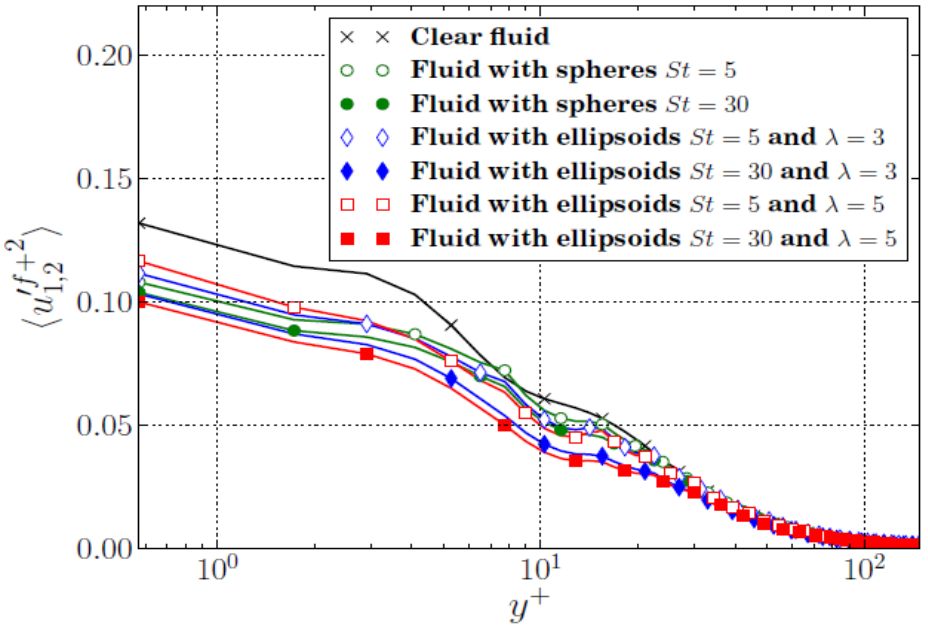

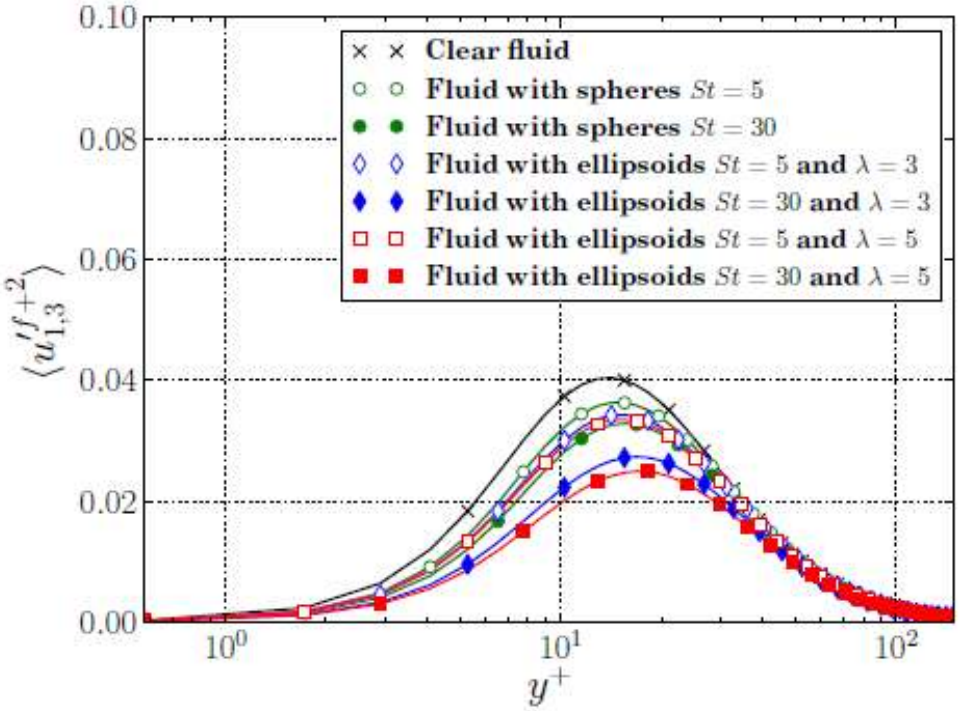

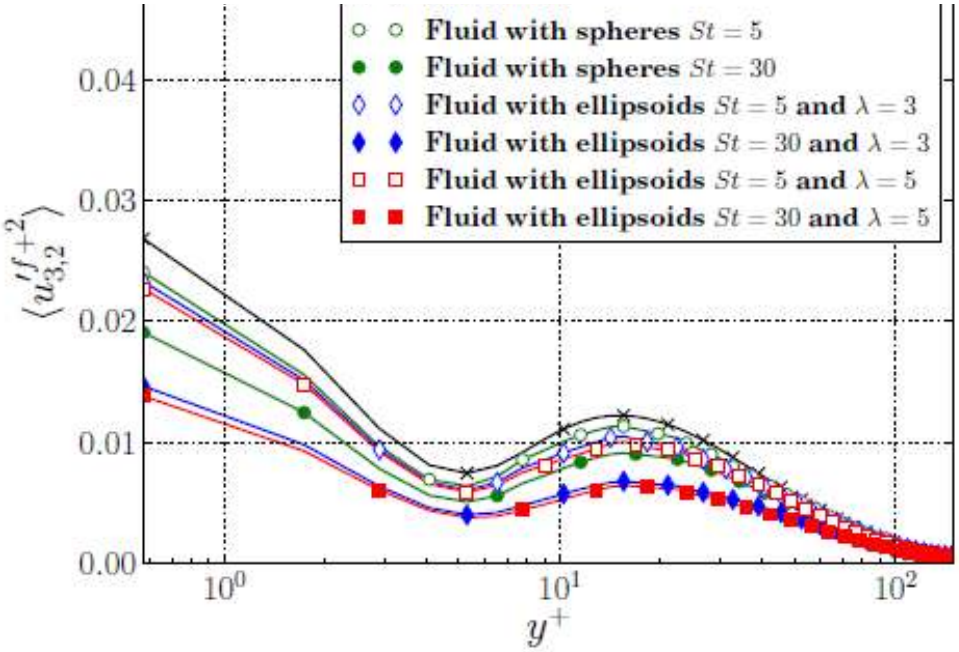

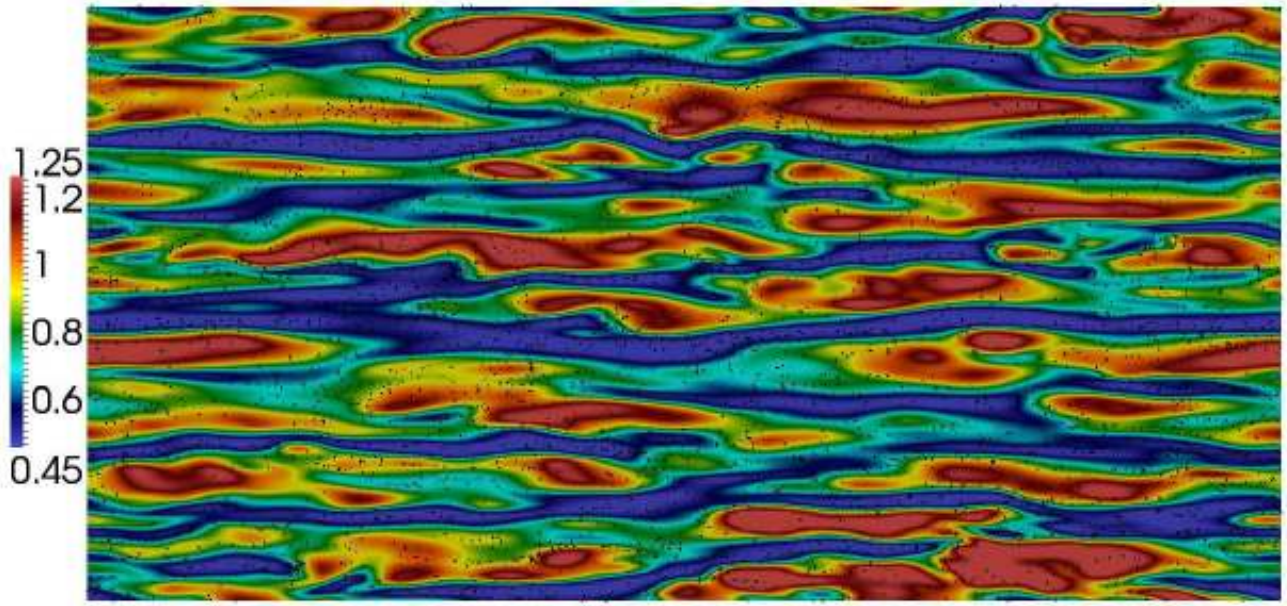

Fig. 28 The instantaneous fluid velocity (indicated by colour) in the stream-wise direction and the distribution of spherical particles with $St = 5$ near the cross-sectional x-z plane at $y^+ = 8$

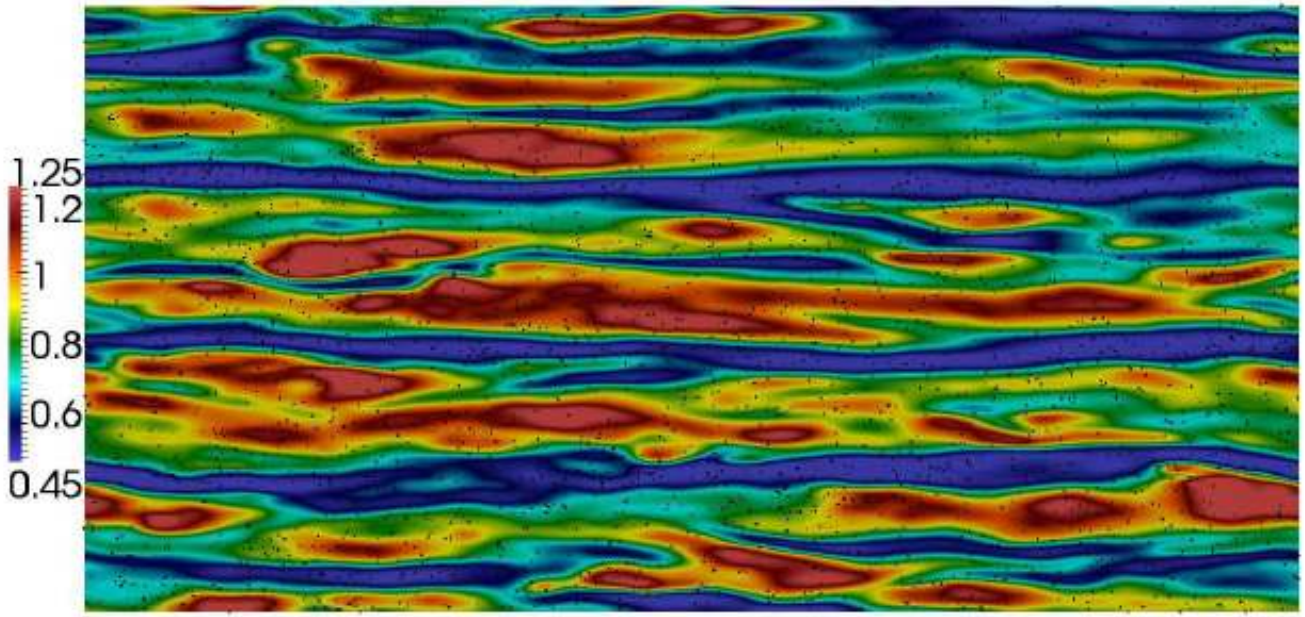

Fig. 29 The instantaneous fluid velocity (indicated by colour) in the stream-wise direction and the distribution of ellipsoids with $St = 30$ and $\lambda = 5$ near the cross-sectional x-z plane at $y^+ = 8$

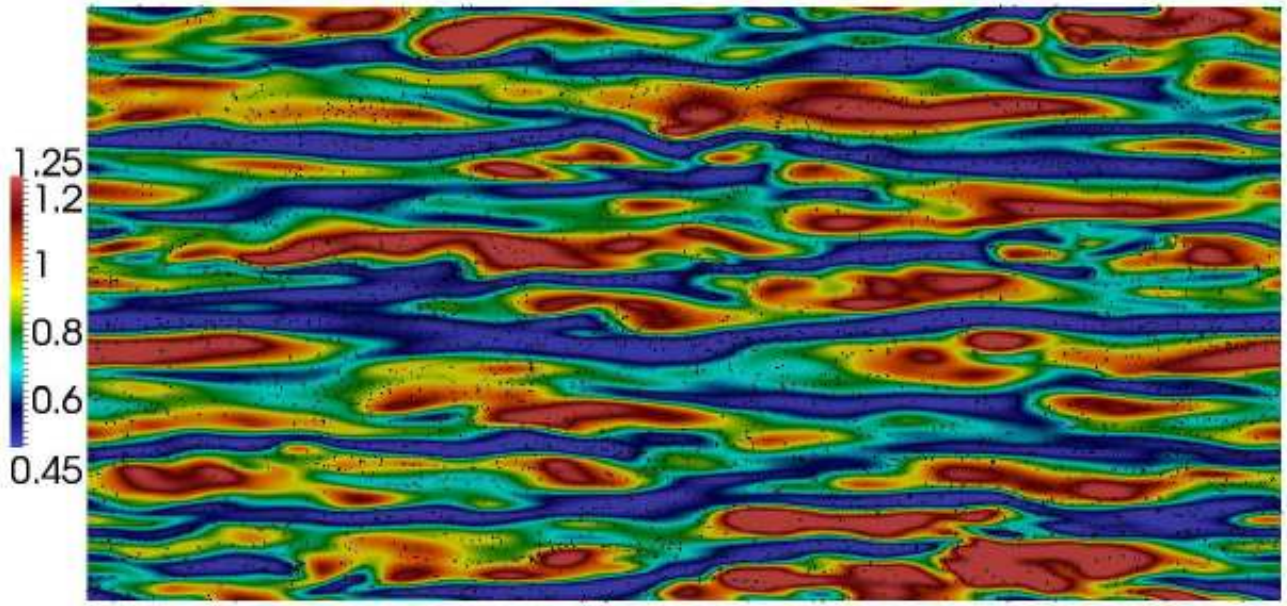

Fig. 28 The instantaneous fluid velocity (indicated by colour) in the stream-wise direction and the distribution of spherical particles with $St = 5$ near the cross-sectional x-z plane at $y^+ = 8$

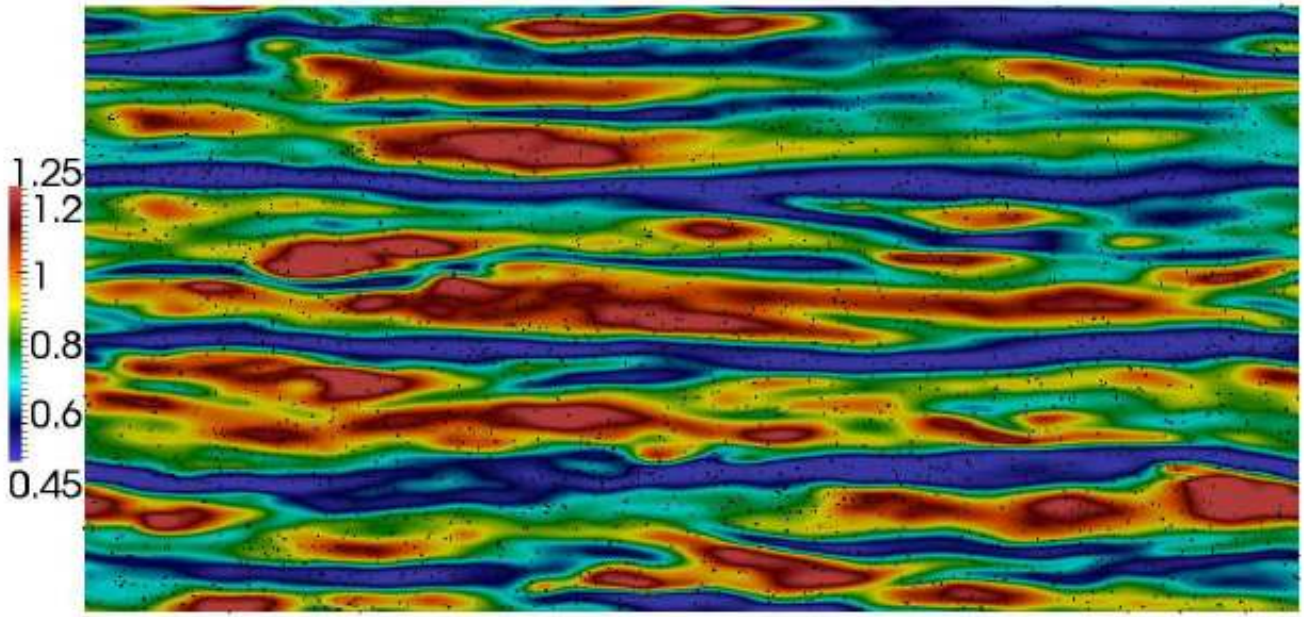

Fig. 29 The instantaneous fluid velocity (indicated by colour) in the stream-wise direction and the distribution of ellipsoids with $St = 30$ and $\lambda = 5$ near the cross-sectional x-z plane at $y^+ = 8$

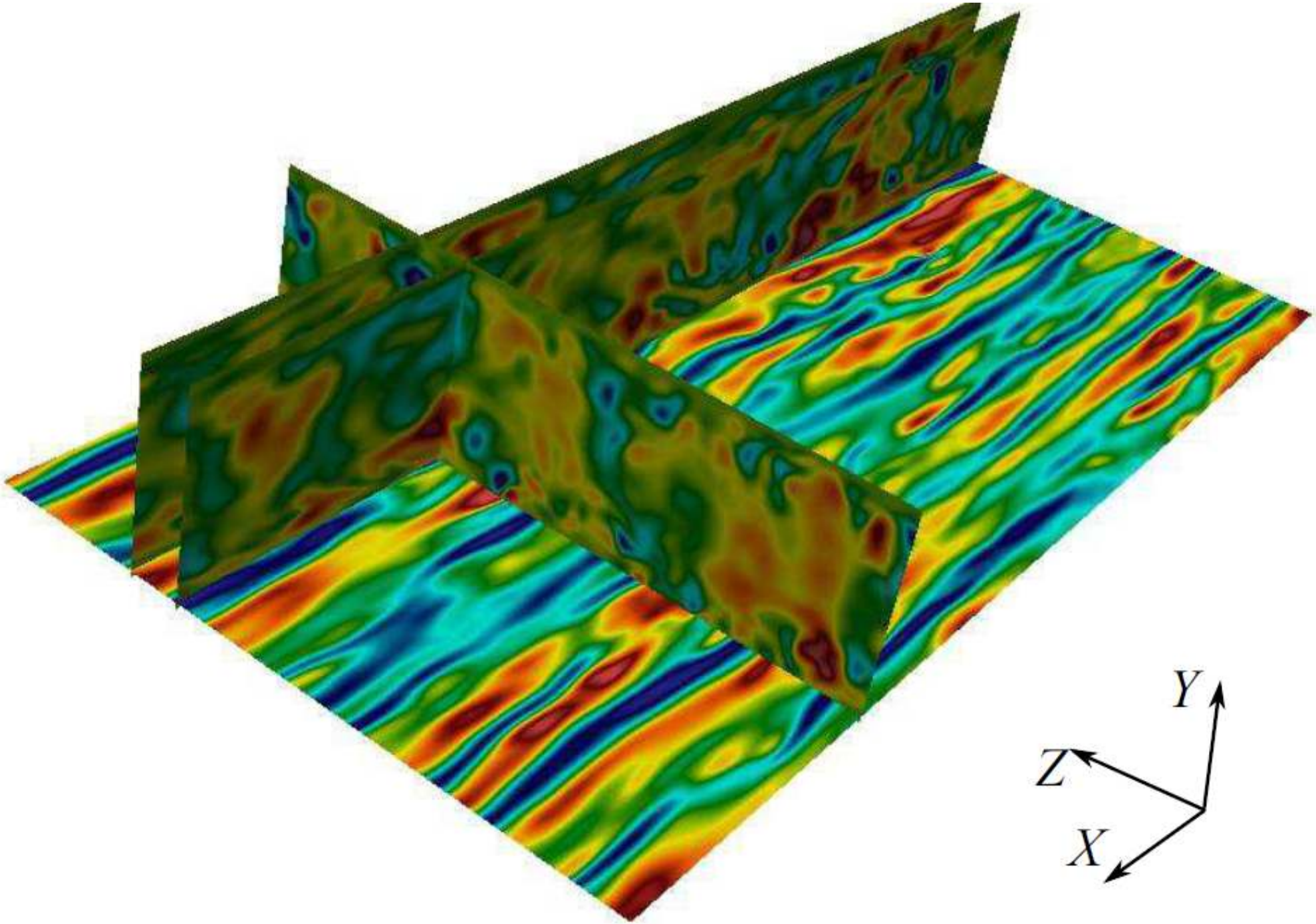

Fig. 1 The contourplot of instantaneous fluid velocity (indicated by colour). The x-z plane on the bottom is coloured by the stream-wise velocity and all the other three planes are coloured by the wall-normal velocity

Where do the particles like to be?

Case with	The area of low-speed fluid flow $(u_1^f - U_1^f < 0)$ at $y^+ = 8.0$	Particles in the low speed area around $y^+ = 8.0$
sphere $(St = 5\ \lambda = 1)$	53.1%	65.60%
sphere $(St = 30\ \lambda = 1)$	53.2%	65.8%
ellipsoid $(St = 5\ \lambda = 3)$	52.1%	64.75%
ellipsoid $(St = 30\ \lambda = 3)$	52.0%	64.4%
ellipsoid $(St = 5\ \lambda = 5)$	53.4%	69.4%
ellipsoid $(St = 30\ \lambda = 5)$	52.3%	59.8%

Table 4 The portion of particles in the low-speed streaks around $y^+ = 8.0$

JPDFs

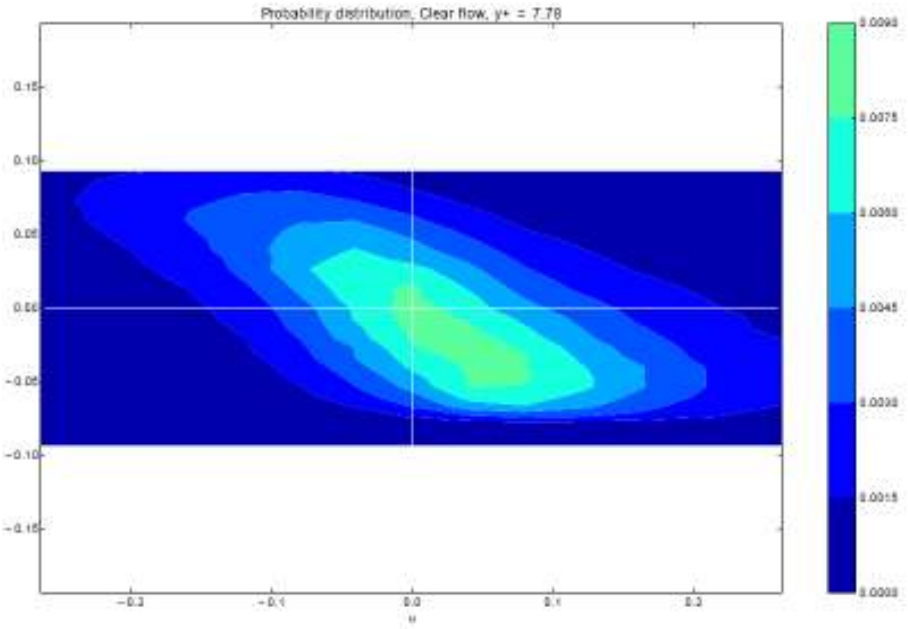
Probability distribution, Clear flow, y+ = 7.78

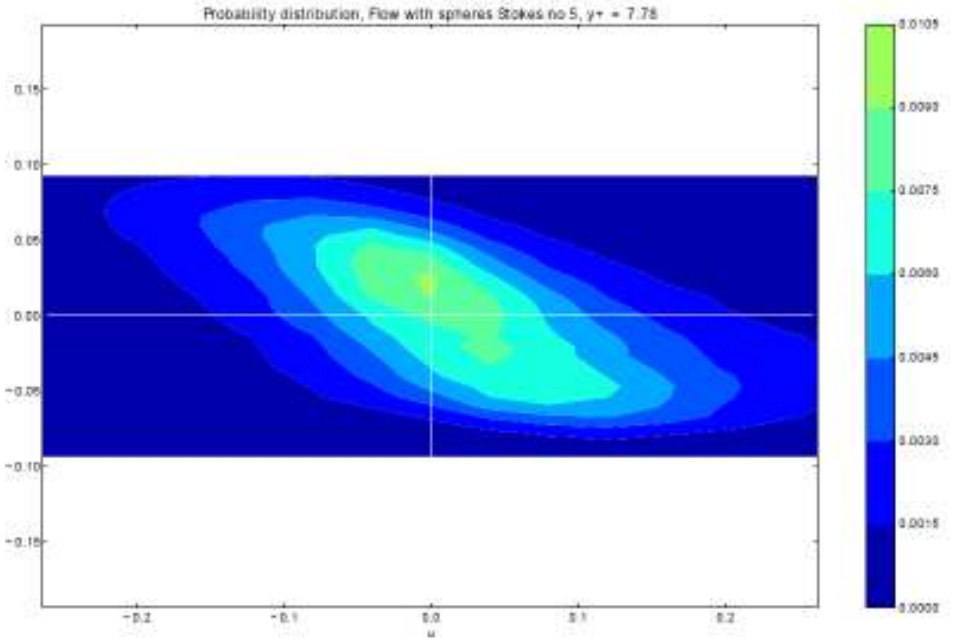
Probability distribution, Flow with spheres Stokes no 5, y+ = 7.78

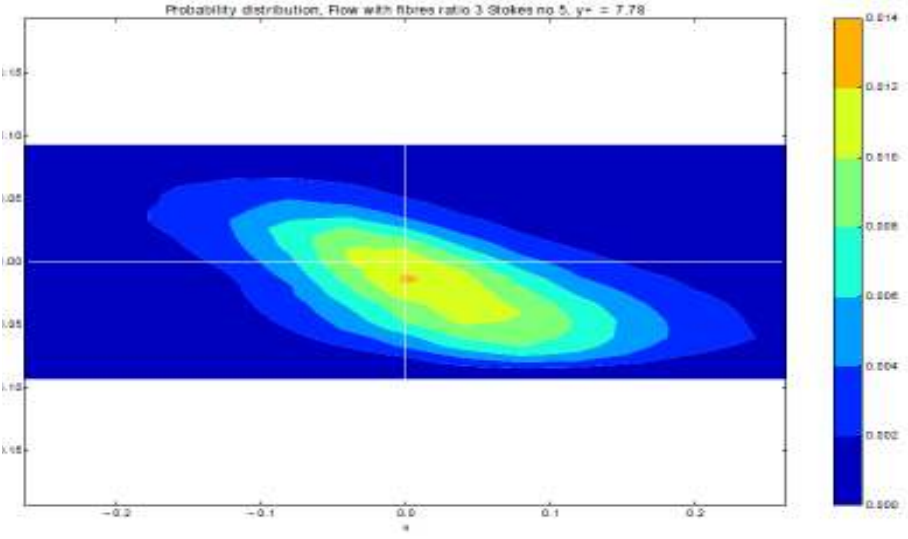
Probability distribution, Flow with fibres ratio 3 Stokes no 5, y+ = 7.78

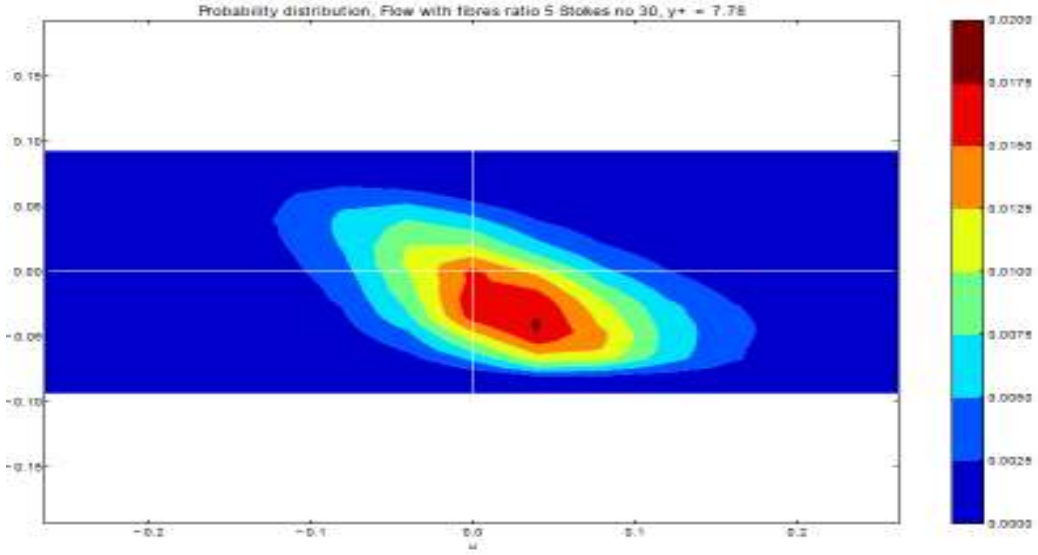
Probability distribution, Flow with fibres ratio 5 Stokes no 30, y+ = 7.78

JPDFs (continued)

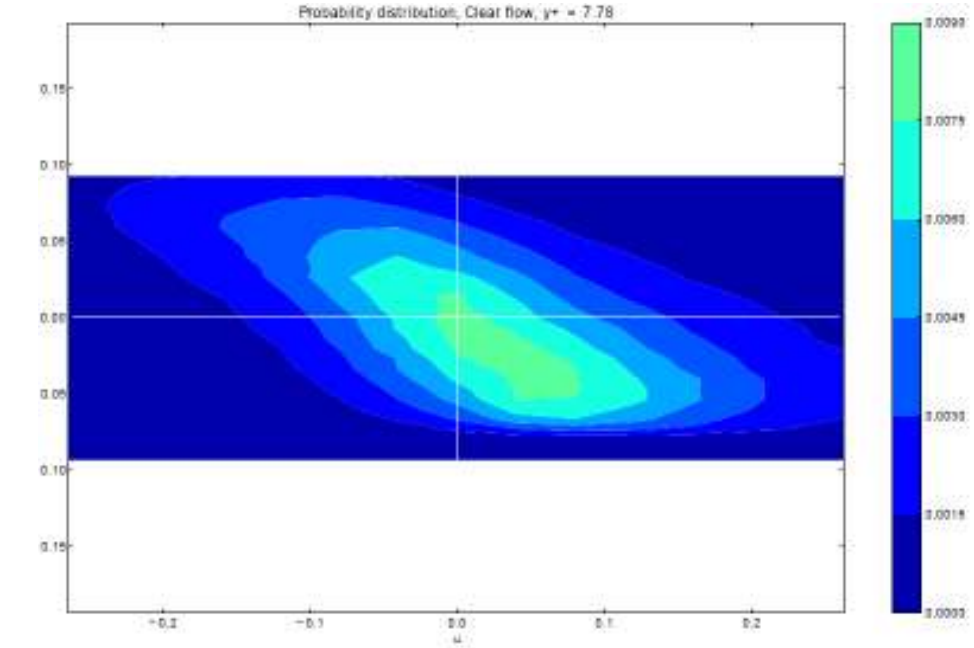

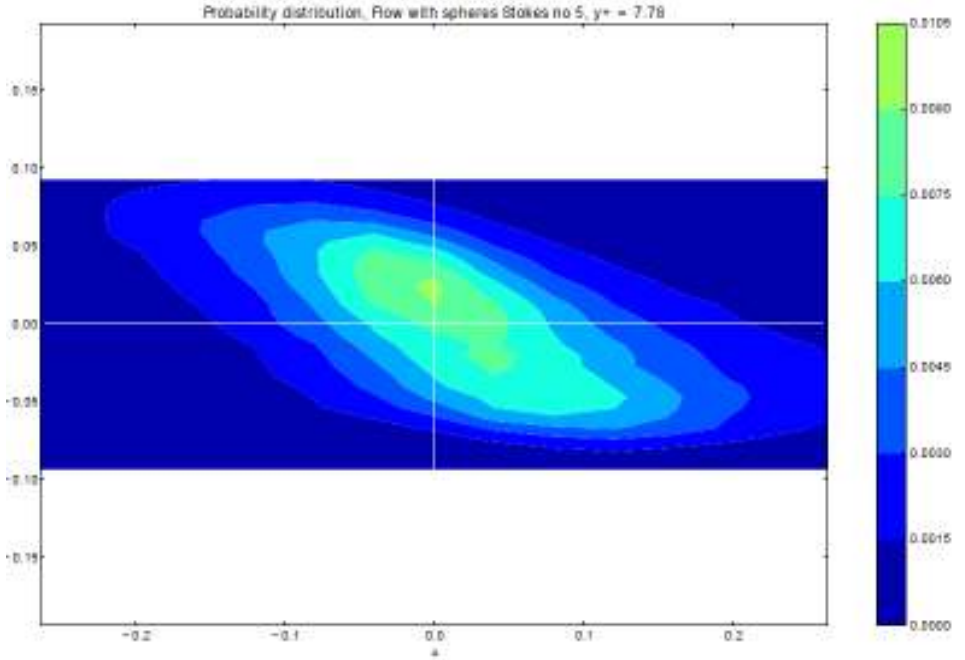

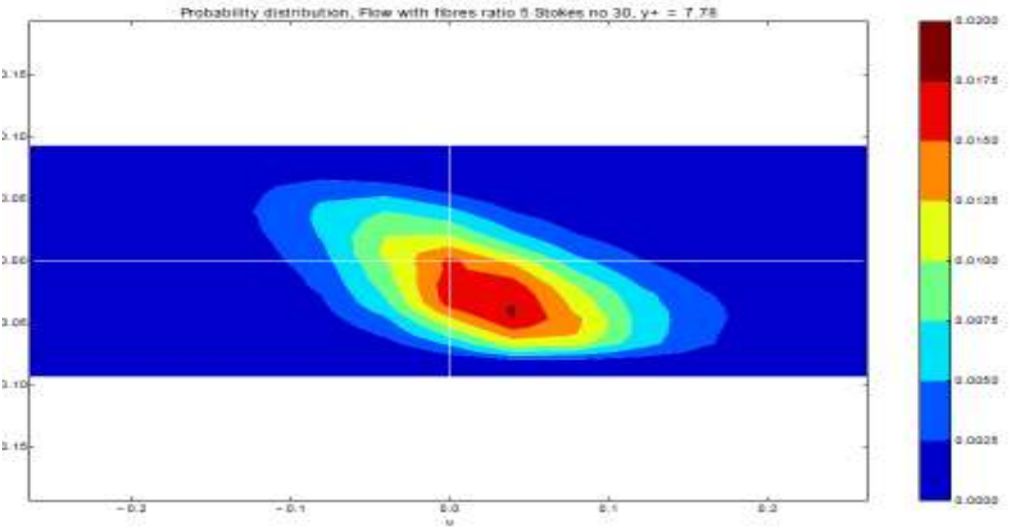

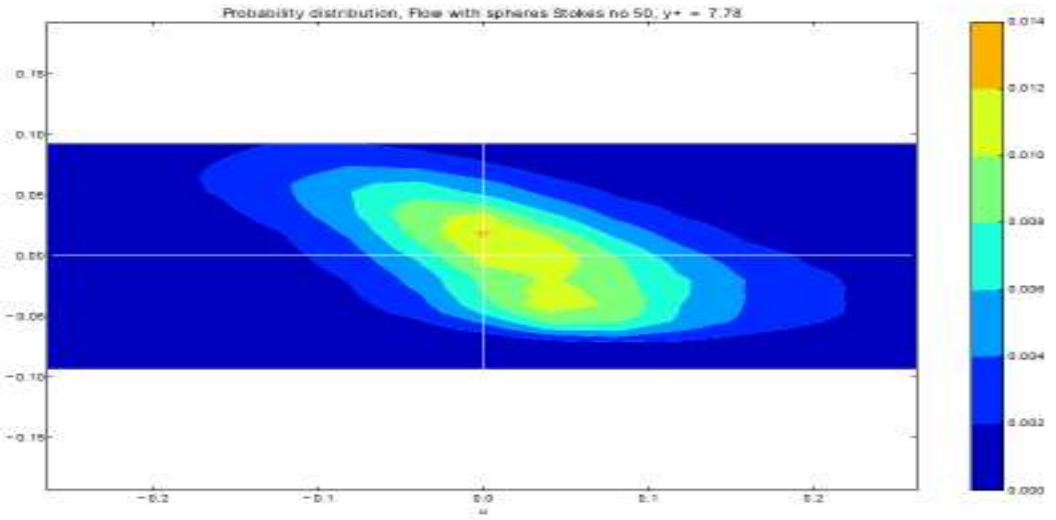

Conclusions

- Effect of dilute solutions not due to viscosity changes.
- Main effect is to change turbulence structures near wall by suppressing ejections.
- Continuity (of flow) implies both sweeps and ejections affected.
- But no continuity for particles – so clustering until collisions and bouncing from wall dominate other effects.
- Maximal effects near Stokes of order unity.
- High inertia ellipsoids pretty much ignore flow.